Available online at www.sciencedirect.com

ScienceDirect

Ceramics International 40 (2014) 1447–1456

CERAMICS INTERNATIONAL

www.elsevier.com/locate/ceramint

Spherical shaped pore structured cermet supports for solid oxide fuel cells

Young Min Park[a], Haekyoung Kim[b,*]

[a]Fuel Cell Project, Research Institute of Industrial Science and Technology, Pohang 790-330, Republic of Korea
[b]School of Materials Science & Engineering, Yeungnam University, Gyeongsan 712-749, Republic of Korea

Received 29 May 2013; received in revised form 3 July 2013; accepted 4 July 2013
Available online 21 July 2013

Abstract

Anode-supported solid oxide fuel cells (SOFC) have been extensively investigated due to their ease of fabrication, robustness, and high electrochemical performance. In this study, anode supported SOFCs are fabricated and characterized as a function of the components in the anode supports. The addition of Fe_2O_3 to NiO–yttria stabilized zirconia (YSZ) anode support tape changes the morphology of the support. Nickel ferrite spinel from the reaction of Fe_2O_3 and NiO during co-firing produces spherical shaped macropores without a change in porosity. SOFCs fabricated by the addition of 0 wt%, 5 wt%, 10 wt%, and 20 wt% Fe_2O_3, exhibit maximum power densities of 2.24 W cm^{-2}, 2.45 W cm^{-2}, 2.38 W cm^{-2}, and 2.09 W cm^{-2}, respectively, at 800 °C with sufficient H_2 fuel. With a lower H_2 flow rate, SOFC fabricated without Fe_2O_3 shows fluctuating and lowered fuel cell performance. SOFC fabricated with 5 wt% Fe_2O_3 shows stable and improved performance. The dense percolation of spherical shaped macropores and a well-connected electrical conduction path, both of which are formed by adding Fe_2O_3, result in lowered charge and mass transfer polarization, which increase the fuel cell performance. However, as a result of the increased charge transfer polarization, the addition of 20 wt% Fe_2O_3 results in Fe diffusion into the anode functional layer and reduces the fuel cell performance. To obtain improved and stable fuel cell performance, the development of spherical shaped macropores is beneficial and the addition of other elements should be considered.

Keywords: Solid oxide fuel cell; Anode supported cell; Anode support; Porous electrode; Nickel iron

1. Introduction

SOFCs are considered to be the most promising energy generation system; they can directly convert various hydrocarbon containing fuels to electrical energy with high efficiency. The development of low cost materials and fabrication processes are the key technical challenges for increasing cell performance and improving the mechanical properties of SOFCs [1–4]. Anode-supported SOFCs, which consist of an Ni–YSZ anode support, Ni–YSZ anode functional layer (AFL), YSZ electrolyte, and cathode, are the most widely used types of SOFC in the current system [5,6]. The tape casting and co-firing method of anode support, AFL and electrolyte, is cost effective and is an easier process for fabricating planar anode supported SOFCs. In order to achieve excellent cell performance in the anode-supported SOFCs, a porous Ni–YSZ anode support has to fulfill the requirements of electronic conductivity, anodic properties, long-term functionality, and high permeability for the fuel gas and the reaction product (by a well-sized and connected porous structure). To improve fuel cell performances, the compositions and components of the Ni–YSZ anode support have been investigated in terms of conductivity and porosity [7–10]. The addition of iron has been reported to be beneficial for improving catalytic activity not only in AFL but also in the support [7]. NiFe has been developed as the reforming and oxidation catalyst in AFL due to the lower activity of iron for carbon formation and better performance in SOFCs with hydrocarbon fuel [9,10]. NiFe has a better matching of its thermal expansion coefficient (TEC), 12–17 × 10^{-6} K^{-1}, with the YSZ electrolyte than does Ni, which has a value of

*Corresponding author. Tel.: +82 53 810 2536; fax: +82 53 810 4628.
E-mail address: hkkim@ynu.ac.kr (H. Kim).

0272-8842/$ - see front matter © 2013 Elsevier Ltd and Techna Group S.r.l. All rights reserved.
http://dx.doi.org/10.1016/j.ceramint.2013.07.028

$15–18 \times 10^{-6}\ K^{-1}$. NiFe also forms extensive solid solutions and intermetallic phases [8]. In terms of processing and performance, Fe, as an additional material, could be a good candidate for anode support.

In this study, iron oxide is added and fabricated into an NiO–YSZ anode support layer tape in order to investigate the effects of iron oxide, which is co-fired with NiO–YSZ AFL and the YSZ electrolyte. The change of morphology of the anode support is characterized and the fuel cell performance is studied here in terms of the amount of iron oxide in the anode support tape.

2. Experimental procedures

Anode supported SOFC was fabricated by a co-firing process in three thin layers; anode support, AFL, and electrolyte. The slurry for the porous support tape consisted of NiO (0.4 μm, High Purity Chemicals), Fe_2O_3 (0.15 μm, High Purity Chemicals), graphite (~5 μm, Carbonix) and an organic binder of polyvinyl butyral (PVB). Each support is coded with the Fe_2O_3 weight ratio to NiO, such as 0 wt% Fe_2O_3 (NiO 65 wt% and YSZ 35 wt%), 5 wt% Fe_2O_3 (NiO 61.75 wt%, Fe_2O_3 3.25%, and YSZ 35 wt%), 10 wt% Fe_2O_3 (NiO 58.5 wt%, Fe_2O_3 6.5%, and YSZ 35 wt%), and 20 wt% Fe_2O_3 (NiO 52 wt%, Fe_2O_3 13%, and YSZ 35 wt%). The starting materials were mixed and ball-milled with zirconia balls (diameter = 10 mm and 5 mm) for 48 h. In order to prepare the AFL tape, NiO (0.1 μm, J.T. Baker Chemical Co) powder and 8 mol% Y_2O_3–stabilized ZrO_2 (YSZ, TZ8Y, Tosoh) powder at a 6:4 weight ratio were mixed and ball-milled with polyvinyl butyral (PVB) binder solution. The YSZ electrolyte tape was prepared with YSZ powder and PVB binder solution. The support, AFL, and electrolyte tapes were laminated under conditions of 40 MPa at 80 °C for 10 min. The laminated tapes with dimensions of 25 cm × 25 cm were fired at 700 °C for 2 h to burn out the graphite, binder, and organic additives. Subsequently, the laminated tapes were sintered at 1370 °C for 3 h in an air atmosphere. A gadonillium doped ceria (GDC) interlayer of ~1 μm was formed on the YSZ electrolyte via aerosol deposition method after the co-firing process. The anode supported cells (ASCs) with NiO–Fe_2O_3–YSZ support (~900 μm)/NiO–YSZ AFL (~15 μm)/YSZ(~10 μm)/GDC (~1 μm) were cut into circles with diameters of 2.6 cm from the co-fired cell. A composite paste with a composition of $La_{0.6}Sr_{0.4}Co_{0.2}Fe_{0.8}O_{3-\delta}$ (LSCF, Seimi Chemicals) and GDC (Anan Kasei) in a 5:5 weight ratio as a cathode was screen-printed on the GDC interlayer of ASC. Subsequently, a paste with pure LSCF was screen-printed on the LSCF and GDC composite cathode in order to improve the current collection. The cathode active area was 1 cm^2. The fabricated cell was assembled and sealed with Cerama bond TM 571 from AREMCO in an alumina jig to measure the current–voltage characteristics and impedances. Pt paste and mesh were used for current collection. The cell was heated to 800 °C over a period of 9 h and anode reduction was performed with 300 cc min^{-1} of 97% H_2–3% H_2O for 3 h. To study the current–voltage characteristics, SOFCs were tested with 300 cc min^{-1} of 97% H_2–3% H_2O and 1000 cc min^{-1} of air at 800 °C and 750 °C with a KIKUSUI PLZ-30F. To characterize the effects of fuel flow rate, SOFCs with an anode support of 0 wt% Fe_2O_3 and 5 wt% Fe_2O_3 were characterized at 700 °C as a function of H_2 flow rates of 500, 250, and 100 cc min^{-1}. Impedance measurements with biases of 0–0.45 V were carried out with a Biologic SP300 in the frequency range of 100 kHz–0.1 Hz with an applied AC voltage amplitude of 100 mV. The anode support layers were characterized using the X-ray diffraction method to investigate the phase formation after co-firing. The pore size distribution and porosity of the anode support after reduction were measured using a mercury porosimeter (Autopore IV, Micromeritics, USA). The microstructures of the SOFCs were characterized via scanning electron microscopy (SEM) using a JSM-6480LV before and after anode support reduction. After the electrochemical performance measurement, the microstructures of the SOFCs were also characterized via SEM.

3. Results and discussion

The starting materials for the anode support consist of NiO, Fe_2O_3 and YSZ. The composition of YSZ is 35 wt% and the sum of NiO and Fe_2O_3 is 65 wt%. Fe_2O_3 is added at ratios of 5 wt%, 10 wt%, and 20 wt% of the sum of the weight ratio of NiO and Fe_2O_3. After co-firing of the anode supported SOFC at 1370 °C for 3 h in an air atmosphere, the XRD patterns of the anode support were determined and are shown in Fig. 1. Peaks of NiO and YSZ can be observed in the anode support with 0 wt% Fe_2O_3. With the addition of Fe_2O_3, the peaks for Fe_2O_3 are not observed, and the peaks for the $NiFe_2O_4$ phase are observed and strengthened with increasing amounts of Fe_2O_3. YSZ and NiO can be seen clearly as shown in Fig. 1. The XRD patterns show that the addition of Fe_2O_3 forms $NiFe_2O_4$ spinels via the reaction with NiO. The single-phase XRD patterns of YSZ indicate the full dissolution of Fe_2O_3 into YSZ grains and/or grain boundaries [11]. The addition of

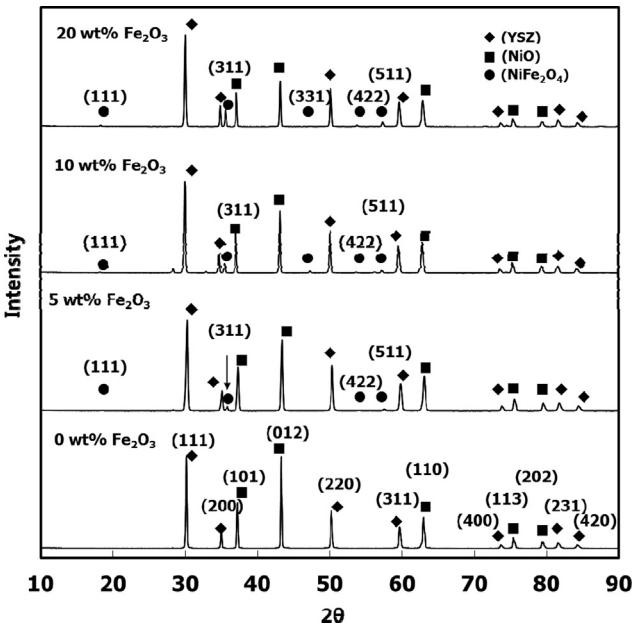

Fig. 1. XRD patterns of support layer.

Fe_2O_3 results in the formation of $NiFe_2O_4$ without any other phase change of the components.

The SEM images of the anode supports before and after reduction are shown in Fig. 2, in which the morphology is shown to have changed due to the additions of Fe_2O_3. The morphological changes can be easily observed in the Ni–NiFe–YSZ support after reduction. The Ni–YSZ and NiO–YSZ supports, as can be seen in Fig. 2(a), show lamellae-shaped pores, which are formed by burning out graphite as a pore former. However, with the addition of only 5 wt% Fe_2O_3

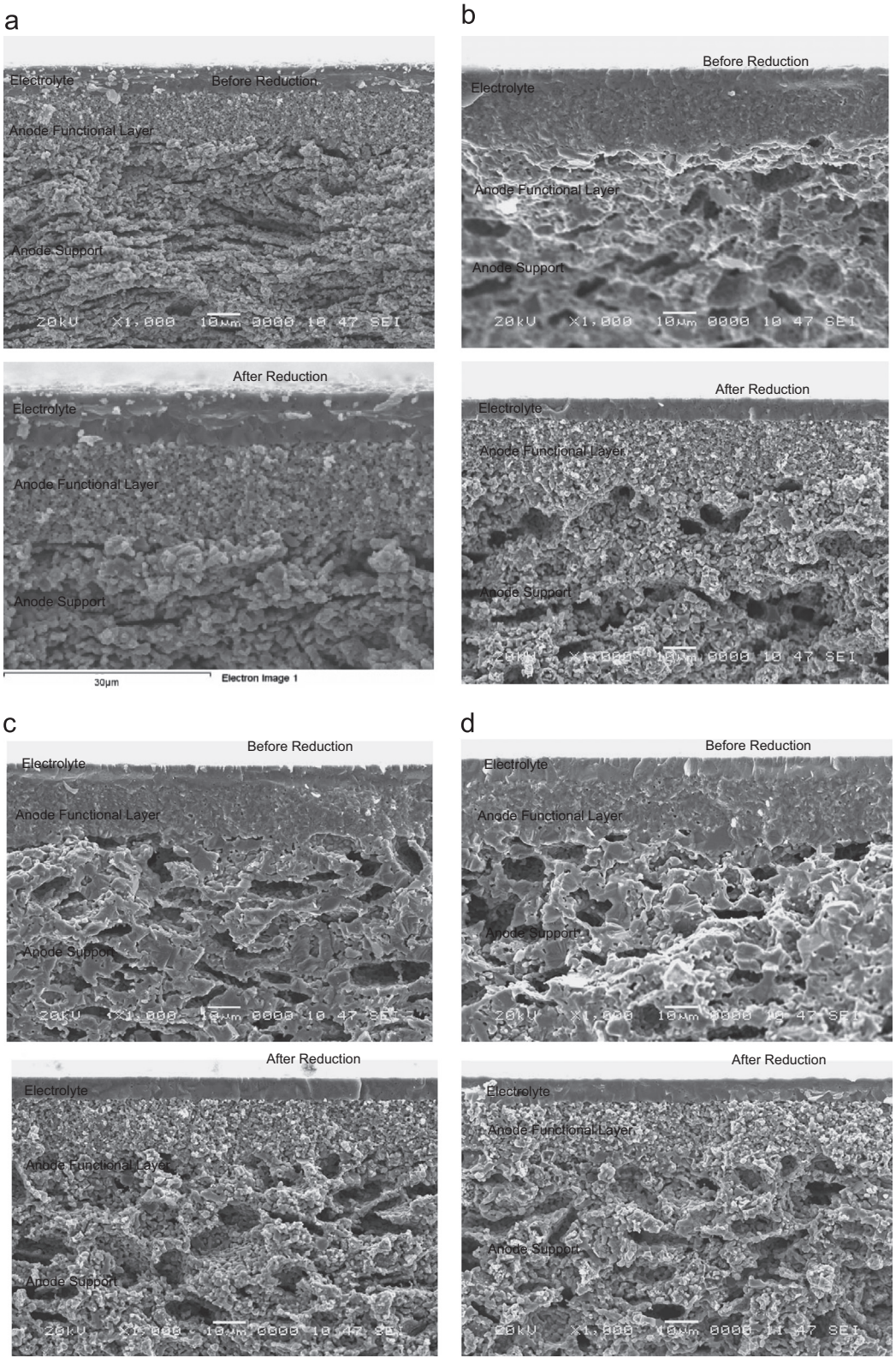

Fig. 2. Cross sectional images of SOFCs with supports of (a) 0 wt% Fe_2O_3, (b) 5 wt% Fe_2O_3, (c) 10 wt% Fe_2O_3 and (d) 20 wt% Fe_2O_3

to a NiO–YSZ support, a morphology of dramatically changed and spherical shaped macropores of ~10 μm can be easily observed with lamellae shaped macropores as shown in Fig. 2 (b), (c), and (d). The morphological changes may be induced by several causes. The lattice parameter of iron oxide doped YSZ may have contracted, which may contribute to the change of the microstructure [11]. However, in this study, the shift of XRD peaks is hard to observe, which means that the microstructural changes are not primarily due to the contraction of YSZ grains.

To analyze the morphological changes, TEM images around the macropores of the anode supports before reduction are characterized, as shown in Fig. 3. Using TEM images and electron dispersive spectroscopy (EDS) analysis, NiO, $NiFe_2O_4$, and YSZ are observed around the spherical shaped macropores, as shown in Fig. 3(a). The presence of $NiFe_2O_4$ (JCPDS # 74-1913, cubic, $a=b=c=0.826$ nm) spinel is proved by the diffraction pattern and the EDS spectra in the TEM dark field images shown in Fig. 3(a). The chemical analysis mappings of Ni, Fe, Zr, and O are shown in Fig. 3(b). The EDS spectra and the chemical mappings show that $NiFe_2O_4$ is formed as a discrete grain (area *C*, spectrum 11) and as a precipitate inside the NiO grain (area *A* and *B*). The inter-diffusion of NiO and Fe_2O_3 at 1370 °C induces the $NiFe_2O_4$ discrete phase and precipitation inside NiO grains. The morphological change with the addition of Fe_2O_3 causes the $NiFe_2O_4$ formation, which results in spherical shaped macropores with lower surface energy driven by the strong inter-diffusion of NiO and Fe_2O_3.

The porosity and pore size distribution were measured after reduction of the supports. The supports have similar porosities of 50.1%, 50.4%, and 48.9% in the 0 wt% Fe_2O_3, 5 wt% Fe_2O_3, and 10 wt% Fe_2O_3, respectively. The fuel cell performances depend on the porosity reported by Zhao's work, where they showed the highest performance in 57% of porosity [12]. However, the additions of Fe_2O_3 lead to changes in the pore size distributions as shown in Fig. 4. The addition of Fe_2O_3 to the support produces macropores with similar porosity. With increasing amounts of Fe_2O_3, the pore size distribution shifts to the larger pore size. The higher gas permeability in the supports with Fe_2O_3 is expected to be affected by the relatively coarse pore channels that are formed

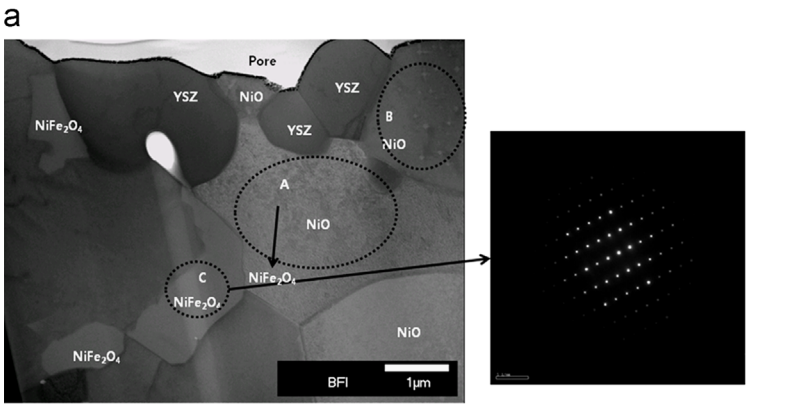

Processing option : All elements analysed

Spectrum	In stats.	O	Fe	Ni	Zr
1	Yes	57.66	28.70	13.64	0.00
2	Yes	50.17	0.89	48.94	0.00
3	Yes	53.26	0.84	0.00	45.90
4	Yes	52.27	0.00	47.73	0.00
5	Yes	61.86	0.00	0.00	38.14
6	Yes	56.77	0.00	0.00	43.23
7	Yes	48.65	0.00	51.35	0.00
8	Yes	44.36	0.65	33.36	21.64
9	Yes	49.62	2.60	47.78	0.00
10	Yes	48.41	0.93	50.66	0.00
11	Yes	58.03	27.85	14.12	0.00
12	Yes	60.45	26.59	12.96	0.00
13	Yes	51.02	2.38	46.60	0.00
Spectrum 14	Yes	46.54	1.64	51.82	0.00
Spectrum 15	Yes	53.20	4.50	42.30	0.00
Mean		52.82	6.51	30.75	9.93
Std. deviation		5.18	11.05	21.19	17.77
Max.		61.86	28.70	51.82	45.90
Min.		44.36	0.00	0.00	0.00

All results in atomic%

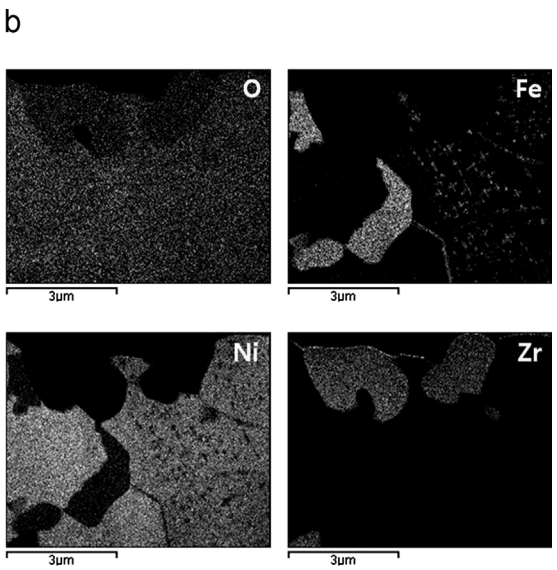

Fig. 3. TEM images surrounding macro-pores (a) dark field images and EDS analysis and (b) chemical analysis mapping.

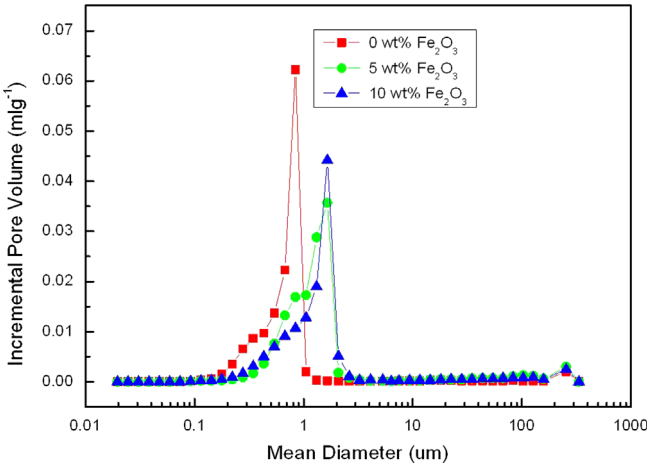

Fig. 4. Pore size distributions as a function of added Fe_2O_3 amounts.

by the formation of spherical shaped macropores and the retention of comparable porosity [13].

The fuel cell performances were characterized with H_2 at 300 cc min^{-1} and air at 1000 cc• min^{-1} and are shown in Fig. 5. The current density value of the cell at 800 °C and 0.7 V are 2.75 A cm^{-2} with 0 wt% Fe_2O_3 support, 2.79 A cm^{-2} with 5 wt% Fe_2O_3 support, and 2.58 A cm^{-2} with 10 wt% Fe_2O_3 support, and 1.99 A cm^{-2} with 20 wt% Fe_2O_3 support. The maximum power densities are 2.24 W cm^{-2}, 2.46 W cm^{-2}, 2.38 W cm^{-2}, and 2.09 W cm^{-2} with 0 wt%, 5 wt%, 10 wt%, and 20 wt% additions of Fe_2O_3, respectively. The fuel cell performances in the low current density range show similar values in SOFCs with 0 wt%, 5 wt%, and 10 wt% Fe_2O_3. However, the fuel cell performances in the high current density range show improvements when 5 wt% and 10 wt% Fe_2O_3 are added to the anode support. The spherical shaped macroporous structures of the anode supports may result in improvement of the fuel cell performance in the high current density range, with the lowered mass transfer polarization. However, the addition of 20 wt% Fe_2O_3 to the NiO–YSZ support decreases the fuel cell performance, from 2.24 W cm^{-2} for the 0 wt% Fe_2O_3 support to 2.09 W cm^{-2} for the 20 wt% Fe_2O_3. Ishihara shows that the addition of a small amount of Fe to Ni in an AFL can drastically decrease the aggregation of Ni under the cell operating conditions, which results in the increments of both the charge transfer and the diffusion process due to the Fe addition [14]. However, the addition of Fe decreases the total electrical conductivity in comparison to that of the pure samples, with an influence on the electrical conductivity of both the grain and the grain boundary [11]. Here, the effects of Fe_2O_3 addition in the anode support can be expected to show the combined effects of increased mass transfer, decreased electrical conductivity, and increased activity due to the Fe activity and the spherical shaped macro pore structure.

Cross-sectional images of the SOFCs after fuel cell performance measurements were produced by SEM equipped with X-ray energy dispersive spectroscope, with images shown in Fig. 6. The line in Fig. 6 (a) shows the Fe element profiles. Diffusions of Fe into the anode functional layer can be

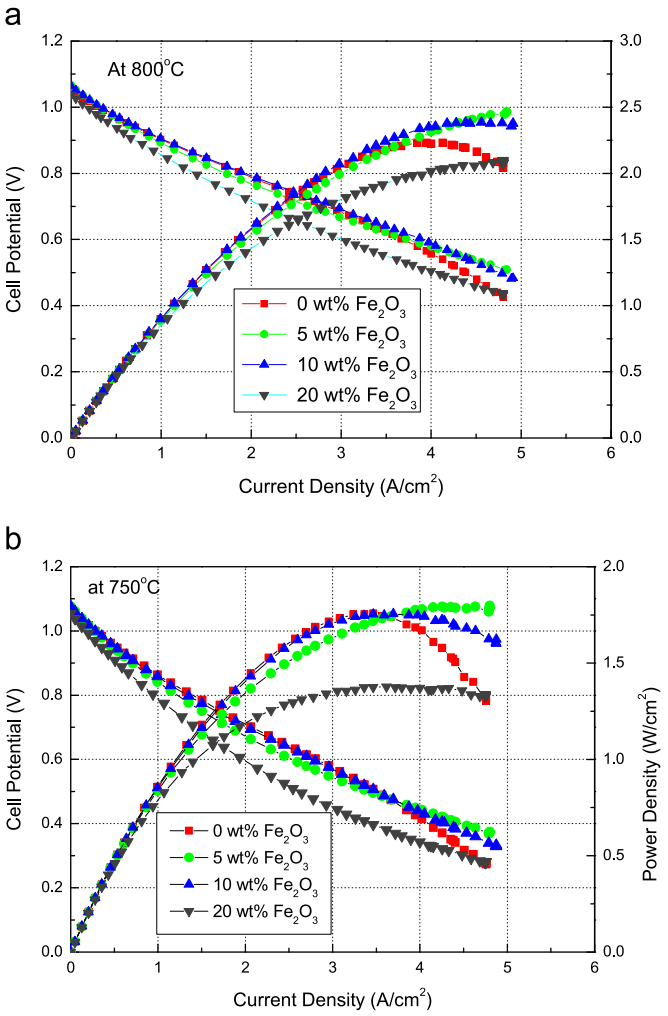

Fig. 5. Fuel cell performances at (a) 800 °C and (b) 750 °C.

observed in the line analysis. The diffusions (the integration of line profiles) become severe as the addition of Fe_2O_3 increases. In this work, the additions of 5 wt% and 10 wt% of Fe_2O_3 to the support layer result in a slight increase in the fuel cell performance. The diffusion of Fe into the anode functional layer may also affect the fuel cell performances; these results are coincident with those of Ishihara's work, in which adding Fe to the anode functional layer resulted in the reported improved fuel cell performances [14]. However, the addition of 20 wt% of Fe_2O_3 to the support layer results in a decrease in the fuel cell performance, which result from severe diffusion of Fe into the anode functional layer.

To investigate the effects of the morphological change with mass transfer, SOFCs with supports of 0 wt% Fe_2O_3 and 5 wt% Fe_2O_3 were characterized as a function of H_2 flow rate at 700 °C. The current–voltage characteristics are shown in Fig. 7. The SOFC fabricated without the addition of Fe_2O_3 to the anode support shows a fluctuation in the fuel cell performance at an H_2 flow rate of 100 cc min^{-1}. The limit of gas diffusion results in the fluctuation and diminution of performance. However, in the SOFC with a support of 5 wt% Fe_2O_3, the fuel cell performances have similar values. The addition of Fe_2O_3 to the support reduces

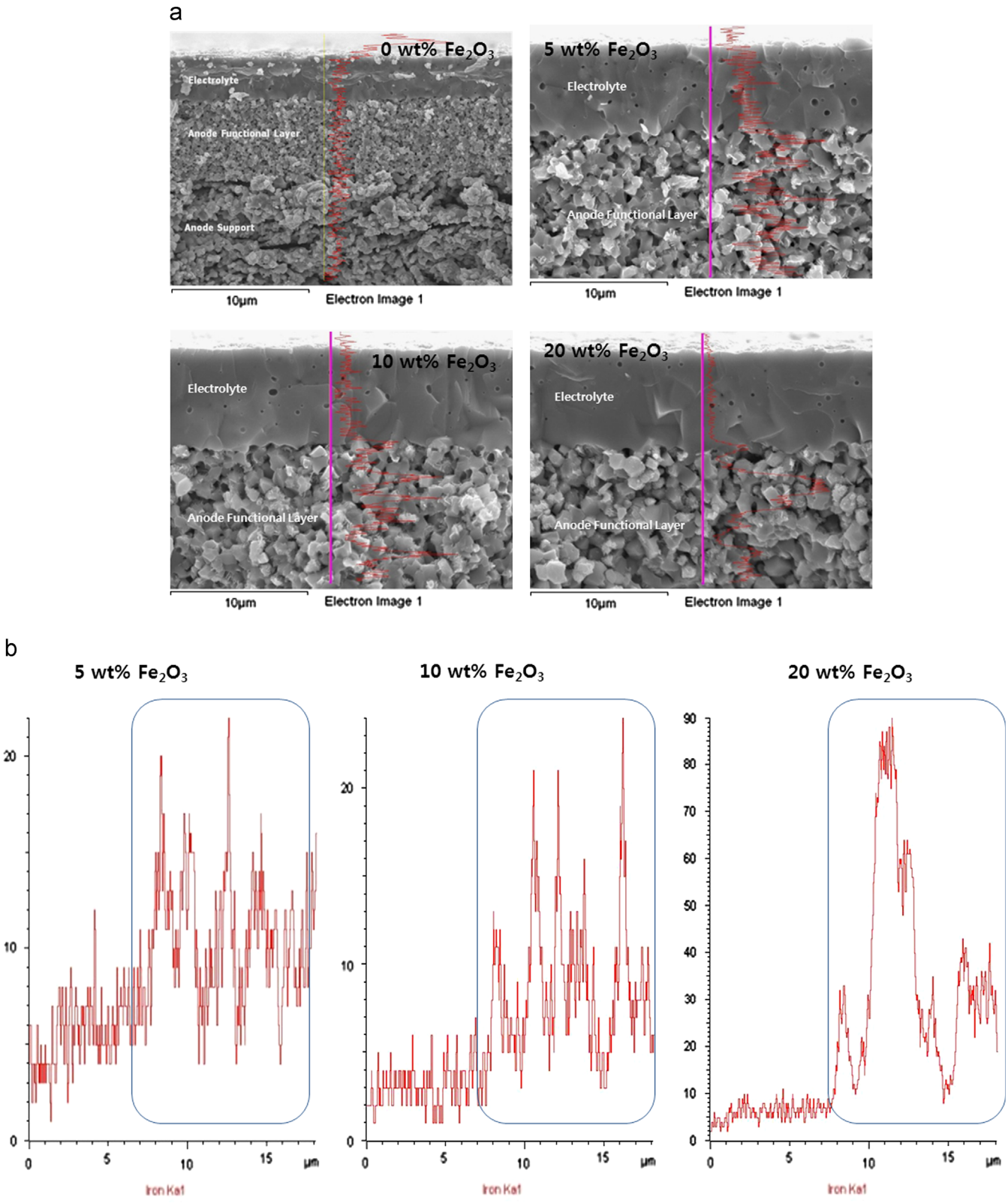

Fig. 6. Microstructure after electrochemical measurements (a) SEM morphologies of SOFCs and (b) EDS Fe line profile in anode functional layer (Box).

the polarization of gas diffusion due to the spherical shaped macropore structure when fuel is supplied in the lower levels. Based on the results of the pore size distribution, as shown in Fig. 4, if there is deficiency of fuel, the fuel cell performance may be more dependent on the pore size distribution rather than on the porosity.

The impedance values of the SOFCs were measured at open circuit voltage (OCV) to study the effects of Fe addition.

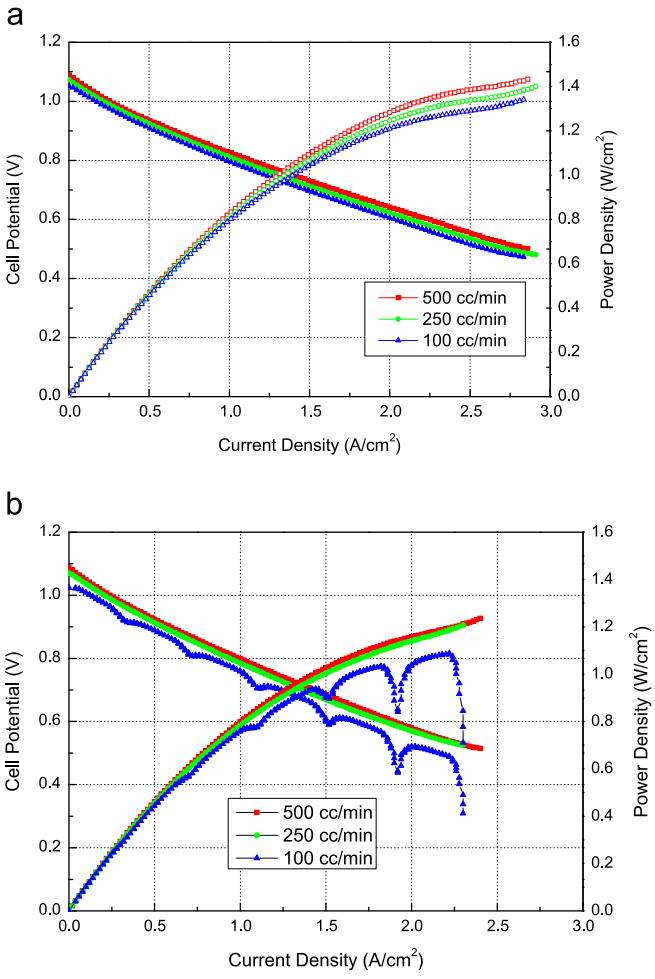

Fig. 7. Fuel cell performances with a flow rate of hydrogen, (a) SOFC with the support of 5 wt% Fe_2O_3 and (b) SOFC with the support of 0 wt% Fe_2O_3.

The equivalent circuit is modeled with five RQ elements, as shown in Fig. 8 [15,16], and the fitting results of the SOFCs match well with the experimental data, as shown in Fig. 9. Fig. 9 shows the impedance values at 800 °C as a function of added Fe_2O_3 in the presence of a sufficient fuel supply. The area specific resistances of the SOFCs are 0.15–0.16 Ω cm^2 with 0 wt%, 5 wt%, and 10 wt% addition of Fe_2O_3. The SOFC with 5 wt% Fe_2O_3 support shows a 0.18 Ω cm^2 area specific resistance. In the fitted model, R0 is from the ohmic resistance of the electrolyte, electrodes, and the connection wires; *L* is the inductance, which is attributed to the platinum current–voltage probes or to the heating elements of the furnace used to heat the sample; (R1Q1) and (R3Q3) correspond to the gas diffusion coupled with the charge transfer reaction and ionic transport; (R2Q2) corresponds to the oxygen surface exchange kinetics and oxygen ion diffusivity at the electrodes; and (R4Q4) and (R5Q5) correspond to the gas diffusion reaction [16–18]. The sum of R1, R2, and R3 is the polarization of the charge transfer and ion diffusivity at the electrode, and is considered to represent the charge transfer polarization of the SOFCs. The sum of R4 and R5 is considered to represent the mass transfer polarization of the SOFCs because R4 and R5

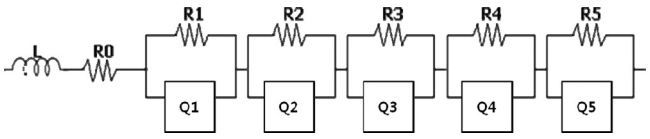

Fig. 8. Equivalent circuit.

correspond to the gas diffusion. The ohmic resistance (R0), charge transfer polarization (sum of R1, R2, and R3), and mass transfer polarization (sum of R4 and R5) are plotted in Fig. 10. The total polarization shows the lowest value in the SOFC with 10 wt% Fe_2O_3 addition. The ohmic resistances of the SOFCs are 0.08–0.1 Ω cm^2 and the charge transfer polarization of the SOFC with 10 wt% Fe_2O_3 shows the lowest value. The mass transfer polarization with 10 wt% Fe_2O_3 shows the highest value with a sufficient fuel supply. The spherical shaped macro pored structure, which formed with the addition of Fe_2O_3, is expected to yield a reduction in the mass transfer polarization. However, with iron addition, the impedances at the OCV show a reduction in charge transfer polarization and an increment in mass transfer polarization. The mass transfer and charge transfer polarizations may be compromised with the spherical shaped macroporous support. Here, the formation of $NiFe_2O_4$ with the addition of 5 wt% and 10 wt% Fe_2O_3 may result in a dense percolation of spherical shaped macropores and a well-connected electrical conduction path, which results in lower charge transfer polarization. These results are coincident with those in Simwonis's work, which showed the improved electrical conductivity in supports with macropores [13]. However, the charge transfer polarization increase for the SOFC with the addition of 20 wt% Fe_2O_3 is shown in Fig. 10. In the SOFC with 20 wt% Fe_2O_3 addition, the diffusion of Fe into the anode functional layer increases the charge transfer polarization and results in lower fuel cell performance [7].

To study the effects of the macro pore structure, the impedance spectra as a function of a H_2 flow rate of 100 cc min^{-1} at 700 °C are shown in Fig. 11. The total polarization is lower in the SOFC with 5 wt% Fe_2O_3 than in the SOFC with 0 wt% Fe_2O_3. With 100 cc min^{-1} of H_2 flow, the SOFC using a support with 5 wt% Fe_2O_3 addition exhibits lowered impedance values, as shown in Fig. 12. With deficient fuel supply, the spherical shaped macropores, formed by adding Fe_2O_3, exhibit the reduced ohmic and mass transfer polarization and the increased charge transfer polarization, which are compromised and reduce the total impedance.

In this work, the addition of Fe_2O_3 to the anode support forms $NiFe_2O_4$ spinels, which produce spherical shaped macropores and result in reduced polarization. After reduction, the pore size distribution in the anode support is shifted to the larger pore size due to the formation of $NiFe_2O_4$ during the co-firing process. The SOFCs with 5 wt% and 10 wt% additions show higher fuel cell performances and especially in the high current density range due to the lowered charge transfer polarization. And with deficient fuel, the lowered mass and ohmic transfer polarization result in the higher and more stable fuel cell performance due to the spherical

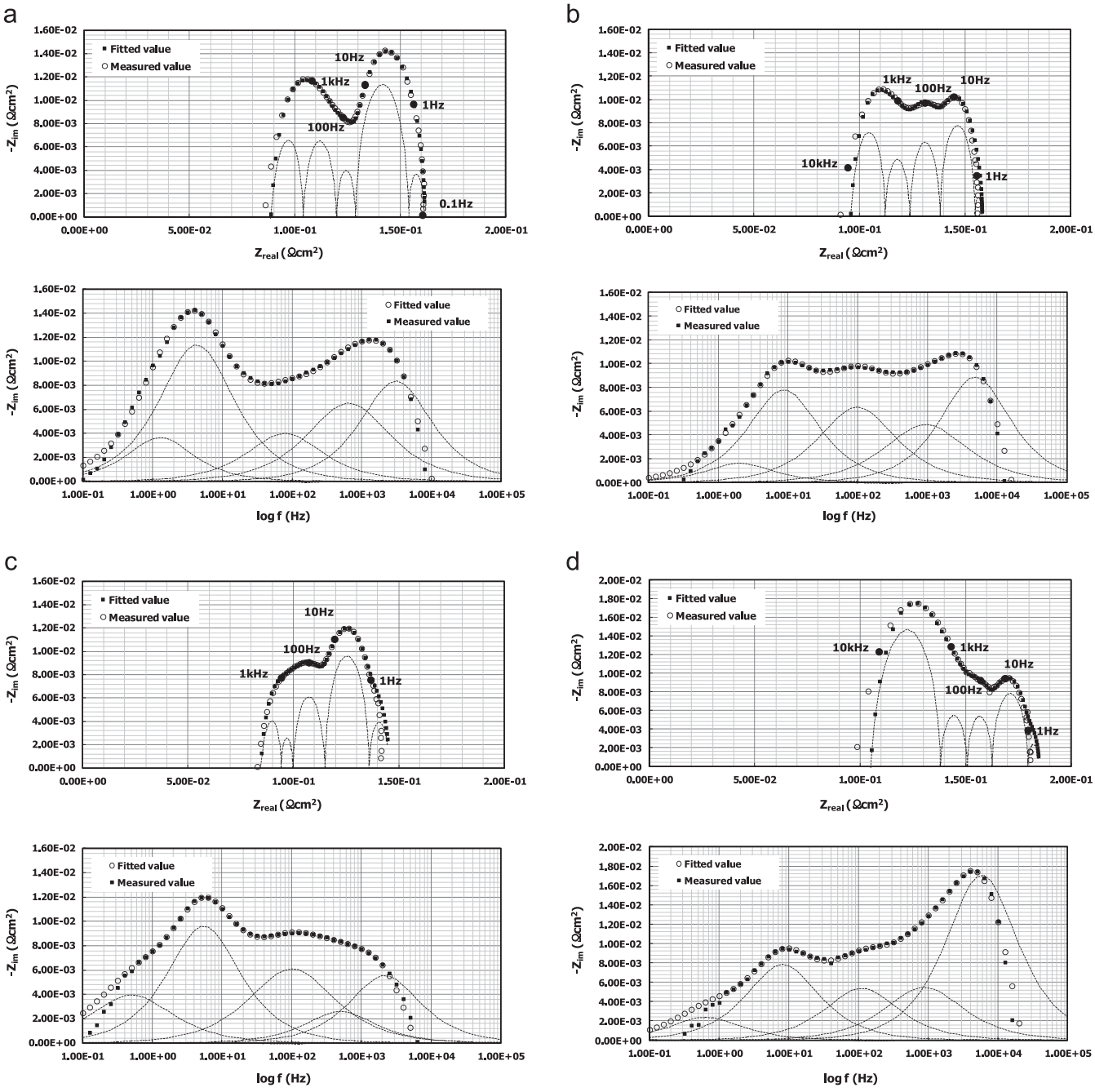

Fig. 9. Impedance Spectra of SOFC at 800 °C and open circuit voltage with support of (a) 0 wt% Fe_2O_3, (b) 5 wt% Fe_2O_3, (c) 10 wt% Fe_2O_3 and (d) 20 wt% Fe_2O_3.

shaped macropores. However, the addition of 20 wt% Fe_2O_3 results in the diffusion of Fe into the anode functional layer, which decreases the fuel cell performance due to increased charge transfer polarization and ohmic resistance. Other elements that may lead to the formation of spherical shaped macropores could be studied to improve the fuel cell performance. Such elements will be beneficial for the H_2 oxidation reaction without incurring the degrading effects of Fe.

4. Conclusions

Anode supported SOFCs were fabricated and characterized in this study as a function of the components of their supports. The addition of Fe_2O_3 to the anode supports of NiO and YSZ changes the morphology of the supports. The formation of $NiFe_2O_4$ spinels from the reaction of Fe_2O_3 with NiO produces spherical shaped macropores without a change in porosity.

The current densities of SOFC at 800 °C and 0.7 V are 2.75 A cm^{-2} with 0 wt% Fe_2O_3 support, 2.79 A cm^{-2} with 5 wt% Fe_2O_3 support, 2.58 A cm^{-2} with 10 wt% Fe_2O_3 support, and 1.99 A cm^{-2} with 20 wt% Fe_2O_3 support. The maximum power densities are 2.24 W cm^{-2}, 2.46 W cm^{-2}, 2.38 W cm^{-2}, and 2.09 W cm^{-2} with 0 wt%, 5 wt%, 10 wt%, and 20 wt% additions of Fe_2O_3, respectively. With the addition of Fe_2O_3, the anode supported SOFCs show higher fuel cell performance in the high current range. The percolation of spherical shaped macropores and the well-connected electrical conduction path with the addition of 5 wt% and 10 wt% Fe_2O_3, result in the lower charge transfer polarization. The SOFC with support of having 5 wt% of Fe_2O_3 also shows stable performance with a deficient H_2 fuel supply and with the lowered ohmic and mass transfer polarization, due to the spherical shaped porous morphology. However, the addition of 20 wt% Fe_2O_3 results in the diffusion of Fe into the anode functional layer and reduces the fuel cell performance due to increased charge transfer polarization. The addition of Fe_2O_3 produces macroporous structures, which are beneficial in attempts to obtain higher fuel cell performances. To control the porosity through the development of spherical shaped macropores, the addition of other elements could be considered.

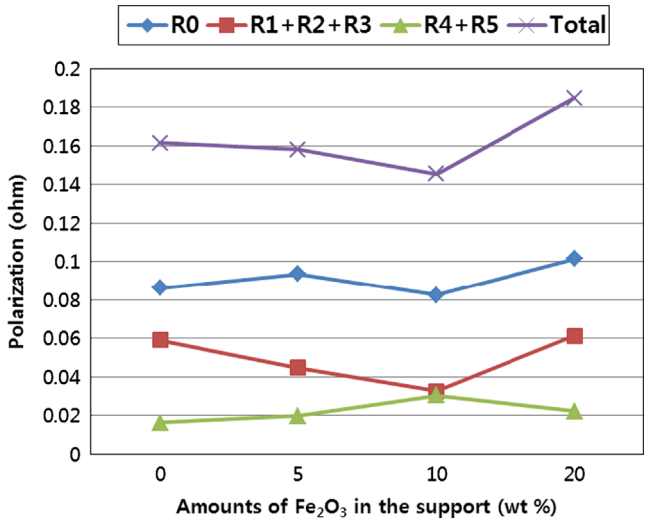

Fig. 10. Polarizations as functional of Fe_2O_3.

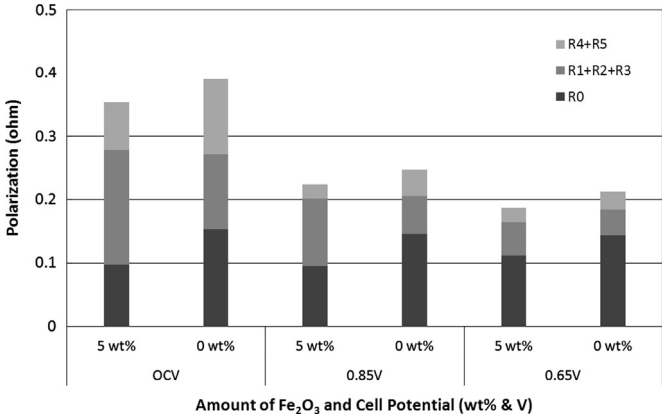

Fig. 12. Polarization from fitted results with 100 cc $min^{-1}H_2$.

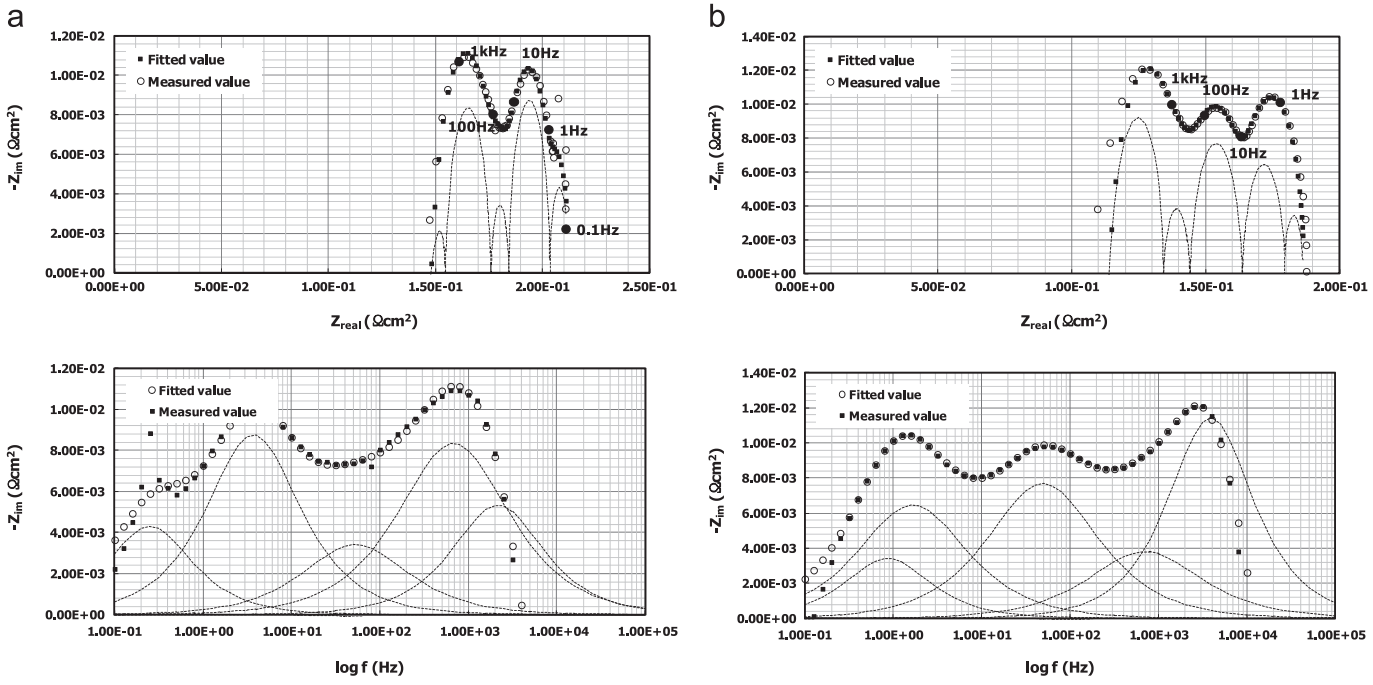

Fig. 11. Impedance of SOFC with 100 cc $min^{-1}H_2$ flow at 700 °C and 0.65 V (a) 0 wt% Fe_2O_3, and (b) 5 wt% Fe_2O_3.

Acknowledgments

This work was supported by the National Research Foundation (NRF) of Korea Grant funded by the Korean Government (MEST) (NRF 2011-0009667).

References

[1] F. Tietz, H.P. Buchkremer, D. Stover, Components manufacturing for solid oxide fuel cells, Solid State Ionics 152–153 (2002) 373–381.
[2] K.H. Kim, Y.H. Park, H. Kim, Fabrication and evaluation of the thin NiFe supported solid oxide fuel cell by co-firing method, Energy 35 (2010) 5385–5390.
[3] N.Q. Minh, Ceramic Fuel Cells, Journal of the American Ceramic Society 76 (1993) 563–588.
[4] S. Hui, J. Roller, S. Yick, X. Zhang, C. Dec'es-Petit, Y. Xie, R. Maric, D. Ghosh, A brief review of the ionic conductivity enhancement for selected oxide electrolytes, Journal of Power Sources 172 (2007) 493–502.
[5] S.C. Singhal, K. Kendall, Solid Oxide Fuel Cell, Elsevier, New York, 2004.
[6] F. Zhao, A.V. Virkar, Dependence of polarization in anode-supported solid oxide fuel cells on various cell parameters, Journal of Power Sources 141 (2005) 79–95.
[7] T. Ishihara, J.W. Yan, M. Shinagawa, J. Matsumoto, Ni–Fe bimetallic anode as an active anode for intermediate temperature SOFC using $LaGaO_3$ based electrolyte film, Electrochimica Acta 52 (2006) 1645–1650.
[8] J.L. Murray, L.H. Bennett, H. Baker, T.B. Massalski, Binary Alloy Phase Diagrams ASM 1 (1986).
[9] A. Atkinson, S. Barnett, R.J. Gorte, J.T.S. Irvine, A.J. McEvoy, M. Mogensen, Advanced anodes for high-temperature fuel cells, Nature Materials 3 (2004) 17–27.
[10] R. Fiuza, M. Silva, J.S. Boaventura, Development of Fe–Ni/YSZ–GDC electrocatalysts for application as SOFC anodes: XRD and TPR characterization and evaluation in the ethanol steam reforming reaction, International Journal of Hydrogen Energy 35 (2010) 11216–11228.
[11] S. Molin, M. Gazda, P. Jasinski, Interaction of yttria stabilized zirconia electrolyte with Fe_2O_3 and Cr_2O_3, Journal of Power Sources 194 (2009) 20–24.
[12] F. Zhao, A Virkar, Dependence of polarization in anode-supported solid oxide fuel cells on various cell parameters, Journal of Power Sources 141 (2005) 79–95.
[13] D. Simwonis, H. ThuÈlen, F.J. Dias, A. Naoumidis, D. StoÈver, Properties of Ni/YSZ porous cermets for SOFC anode substrates prepared by tape casting and coat-mix® process, Journal of Materials Processing Technology 92–92 (1999) 107–111.
[14] T. Ishihara, H. Zhong, Effects of Fe addition on the surface reaction of the anode of intermediate temperature solid oxide fuel cells, Scripta Materialia 65 (2011) 108–111.
[15] A. Leonide, V. Sonn, A. Weber, E. Ivers-Tiffee, Evaluation and modelling of the cell resistance in anode supported solid oxide fuel cells, ECS Transaction 7 (2007) 521–531.
[16] A. Leonide, V. Sonn, A. Weber, E. Ivers-Tiffee, Evaluation and modeling of the cell resistance in anode-supported solid oxide fuel cells, Journal of the Electrochemical Society 155 (2008) B36–B41.
[17] A. Weber, Impedance spectroscopy as a diagnosis tool for SOFC stacks and systems, in: Proceedings of the International Symposium Diagnostics Tools Fuel Cell Technologies, 2009.
[18] H. Schichlein, A.C. Muller, M. Voigts, A. Krugel, E. Ivers-tiffee, Deconvolution of electrochemical impedance spectra for the identification of electrode reaction mechanisms in solid oxide fuel cells, Journal of Applied Electrochemistry 32 (2002) 875–882.